Journal of Southeast University (English Edition) Vol. 35, No. 1, pp. 64 - 71 Mar. 2019 ISSN 1003—7985

ESO-based decoupling control with multi-objective optimization for boiler-turbine unit

Zhu Jianzhong[1,2] Wu Xiao[1] Shen Jiong[1]

([1]Key Laboratory of Energy Thermal Conversion and Control of Ministry of Education, Southeast University, Nanjing 210096, China)
([2]School of Electric Power Engineering, Nanjing Institute of Technology, Nanjing 211167, China)

Abstract: A model-assistant extended state observer (MESO)-based decoupling control strategy is proposed for boiler-turbine units in the presence of unknown external disturbance and model-plant mismatch. For ease of implementation, the decoupling compensator is reduced to the proportion integration (PI) decoupler with the frequency domain analysis, where the decoupling error in collusion of uncertainties and disturbances can be estimated by the proposed MESO and then compensated. To decrease the sensitivity of the dynamic error for the decoupling control and fulfill various requirements of constraints, such as safety operation, energy conservation, emission reduction, etc., the plant is transmitted through a scheduled steady state region which is achieved from the optimized reference governor in advance. Simulation results show that the proposed control strategy can well suppress various disturbances including a decoupling error, and multi-objective optimization can meet multiple requirements with the premise of safety production.

Key words: boiler-turbine unit; extended state observer (ESO); decoupling control; multi-objective optimization
DOI: 10.3969/j.issn.1003-7985.2019.01.010

With the growth of Chinese large-scale renewable energy grid combinations, the dependence on traditional power generation is increased, and higher requirements have been put forward, such as disturbance rejection ability[1]. Due to the existence of tightly coupled, multivariable, large-scale factors of the boiler-turbine unit and the existence of time-varying parameters, large nonlinearities, unknown modelling errors, disturbances, and non-minimum phases in dynamic models, we need a practical scheme to meet these challenges.

Due to the large nonlinearity of the system, when the load demand changes, the conventional proportion integration differentiation (PID) control cannot transmit the output power to the desired value quickly and overshoot is inevitable[2]. In order to solve the large-scale nonlinearity, Chen et al.[3] proposed a gain-scheduled controller design, where the control law was formed by the parameter-dependent nonlinear state-feedback control. From the simulation, the gain-scheduled control design can achieve a smooth output response at the expense of the response speed. Fuzzy PID[4] is a powerful method, which can deal with the nonlinearity by using multiple models. Another conventional control strategy is the loop shaping H_∞ approach, which is applied to the boiler-turbine unit by Tan et al[5]. The obtained controller from the loop shaping is reduced to the PID structure, which plays a dual role of decoupling and feedback controller.

Over the years, model predictive control (MPC) has received extensive attention from researchers in process control, including many successful applications in boiler-turbine control[6-7]. The greatest attraction of MPC[8] is that the current control input is achieved by the prediction of the future dynamic behavior of the system and optimized in a sampling period. Also, the constraints can be explicitly solved. Due to the heavy burden of calculation, Fu et al.[8] stated that MPC cannot be applied to the underlying control of the distributed control system (DCS). So, a hierarchical optimization MPC[9] for the boiler-turbine unit is proposed, where the heavy computing burdens are brought to the top layer. In a newly published article[10], the authors tried to apply the extended state observer(ESO) to fuzzy MPC, and the simulation shows that the closed-loop response has the capability of disturbance rejection. What needs to be explained is that current MPC often adopts linear matrix inequality (LMI) to optimize the algorithm, and the above mentioned methods are mainly conducted on the study of stability but ignore the difficulties of implementation.

In this paper, we present a decoupling-based ESO for the well-known boiler-turbine unit, where the decoupling compensator is simplified to a PI decoupler for the ease of implementation. Conventional active disturbance rejection control (CADRC) proposed by Han[11] is considered as an efficient method to deal with disturbance and uncertainties for the system control design. Moreover, it does not depend on the exact mathematical model. For the boiler-turbine unit with non-minimal phase (NMP) and frequency load regulation, the CADRC achieves less over-shoot

Received 2018-08-29, **Revised** 2018-12-21.

Biographies: Zhu Jianzhong (1981—), male, Ph. D. candidate; Shen Jiong (corresponding author), male, doctor, professor, shenj@seu.edu.cn.

Foundation item: The National Natural Science Foundation of China (No. 51576041, 51506029).

Citation: Zhu Jianzhong, Wu Xiao, Shen Jiong. ESO-based decoupling control with multi-objective optimization for boiler-turbine unit[J]. Journal of Southeast University (English Edition), 2019, 35(1): 64 - 71. DOI: 10.3969/j.issn.1003-7985.2019.01.010.

tracking performance with difficulty. A model-assisted ADRC (MADRC)[12-13] is illustrated as an effective measure to cope with the NMP, and the ESO is designed on the known model information rather than the cascade integral model.

During the implementation of the control scheme, the first problem that needs to be solved is the safety operation for both the decoupling error and the production. The application of the MPC-based disturbance observer (DOB)[14] in the process control has gained much attention, where the MPC is designed to meet the constraint in the upper layer. As an alternative, Zhao et al.[15] provided a particle swarm optimization (PSO) for the objective function. Motivated by the idea of Zhao et al.[15], we propose a nonlinear multi-objective optimization for set-point acquisition.

1 Dynamics of Boiler-Turbine Unit

The well-known oil-fired boiler-turbine unit[7] proposed by Astrom and Bell in 1987, with a rated power of 160 MW and 3-inputs 3-outputs, is a highly nonlinear, strong coupling model, which is widely used in the control design by researchers.

The mathematical description of the system is given as follows:

$$\left.\begin{aligned}\dot{x}_1 &= -0.001\ 8u_2x_1^{9/8} + 0.9u_1 - 0.15u_3\\ \dot{x}_2 &= (0.073u_2 - 0.016)x_1^{9/8} - 0.1x_2\\ \dot{x}_3 &= (141u_3 - (1.1u_2 - 0.19)x_1)/85\end{aligned}\right\} \quad (1)$$

where x_1 denotes the drum pressure, kg/cm^2; x_2 denotes the electric output, MW; and x_3 denotes the fluid density, kg/m^3. The inputs u_1, u_2 and u_3 are the valve positions for fuel flow, steam control, and feedwater flow, respectively.

The outputs of the model are formulized as

$$\left.\begin{aligned}y_1 &= x_1\\ y_2 &= x_2\\ y_3 &= 0.05(0.130\ 73x_3 + 100a_{cs} + q_e/9 - 67.975)\end{aligned}\right\} \quad (2)$$

where y_3 is the drum water level, m; a_{cs} and q_e are the steam quality and evaporation rate, respectively, kg/s; and they are given as

$$a_{cs} = \frac{(1 - 0.001\ 538x_3)(0.8x_1 - 25.6)}{x_3(1.039\ 4 - 0.001\ 2304x_1)}$$

$$q_e = (0.854u_2 - 0.147)x_1 + 45.59u_1 - 2.514u_3 - 2.096$$

Tab. 1 provides the typical operating points of the boiler-turbine unit. The typical operating point 4# is usually chosen to linearize the model.

Tab. 1 Typical operating points of the model

Operating condition	x_1^0/(kg · cm^{-2})	x_2^0/MW	x_3^0/(kg · m^{-3})	u_1^0/%	u_2^0/%	u_3^0/%	y_3^0/m
1#	75.6	15.27	299.6	15.6	48.3	18.3	-0.97
2#	86.4	36.65	324.4	20.9	55.2	25.6	-0.65
3#	97.2	50.52	385.2	27.1	62.1	34.0	-0.32
4#	108.0	66.65	428.0	34.0	69.0	43.3	0
5#	118.8	85.06	470.8	41.8	75.9	54.3	0.32
6#	129.6	105.8	513.6	50.5	82.8	66.3	0.64
7#	135.4	127.0	556.4	60.0	89.7	79.3	0.98

2 Control Design

The model that we need to design is a 3-input 3-output multivariable system, where the strong coupling feature makes the design more complex. If one only applies the decoupling controller to the plant, the model uncertainties will deteriorate the control performance. In this paper, the decoupling error can be estimated by the ESO outside the decoupler and compensated by the feedback controller. With the help of ESO, the selection of the decoupling method is flexible, that is, it becomes insensitive to the model uncertainties.

2.1 Decoupling design

A dynamic decoupling approach proposed by Garrido et al.[16] is validated as an efficient way for the boiler-turbine unit. In this section, a modified decoupling strategy is proposed.

Reconsidering the typical operating point, the nominal transfer matrix $\boldsymbol{G}_n(s)$ is calculated as

$$\boldsymbol{G}_n(s) = \frac{\boldsymbol{Y}(s)}{\boldsymbol{U}(s)} = \frac{1}{398.6s+1}\begin{bmatrix} 358.7 & \dfrac{249.1}{10s+1} & \dfrac{0.011\ 3(34.57s+1)(258.33s-1)}{s}\\ -139.1 & \dfrac{44.96(1\ 255.3s+1)}{10s+1} & \dfrac{0.002\ 2(1\ 428.6s+1)(65.15s-1)}{s}\\ -59.79 & \dfrac{-41.49}{10s+1} & \dfrac{-0.009\ 7(282.57s+1)(2.03s-1)}{s}\end{bmatrix}^{\mathrm{T}}$$

where a right-half-plane (RHP) zero exists in each element of the third row (y_3), and a common large inertial item exists in each element. With the aid of the desired open-loop transfer matrix,

$$\boldsymbol{Q}(s)=\boldsymbol{G}_{\mathrm{n}}(s)\cdot\boldsymbol{D}(s)=\begin{bmatrix} q^{(1)}(s) & 0 & 0 \\ 0 & q^{(2)}(s) & 0 \\ 0 & 0 & q^{(3)}(s) \end{bmatrix} \tag{3}$$

The decoupling controller is achieved by

$$\boldsymbol{D}(s)=\boldsymbol{G}_{\mathrm{n}}(s)^{-1}\cdot\boldsymbol{Q}(s) \tag{4}$$

The design of the diagonal element in $\boldsymbol{D}(s)$ is the main issue of this section. Considering the dynamic behavior of each loop, the desired open-loop transfer function can be expressed as

$$q^{(i)}(s)=k^{(i)}\cdot\bar{q}^{(i)}(s)\cdot\frac{1}{s} \tag{5}$$

where $k^{(i)}$ represents the loop gain; the rational transfer function $\bar{q}^{(i)}$ is determined by the not cancelable dynamics in $\boldsymbol{G}_{\mathrm{n}}(s)$, such as RHP zeros, and the function of the integral action is used to shape the loop transfer function at low frequencies. It should be noted that the constructed $q^{(i)}(s)$ is used as the assisted model to design the ESO of ADRC, so a preferred second-order transfer function should be adopted. An additional low-pass filter can be a good choice to complete the order of the diagonal element, of which the cut-off frequency is judged from the dynamic characteristic. The well-designed desired loop transfer matrix with the diagonal form is shown as

$$\boldsymbol{Q}(s)=\begin{bmatrix} \dfrac{0.04}{s(2s+1)} & 0 & 0 \\ 0 & \dfrac{0.08}{s(2s+1)} & 0 \\ 0 & 0 & \dfrac{0.053s+0.001}{s^2} \end{bmatrix} \tag{6}$$

From Eq. (6), there is no doubt that RHP poles exist in the decoupler $\boldsymbol{D}(s)$ caused by the presence of RHP zeros in $\boldsymbol{G}_{\mathrm{n}}(s)$, which leads to an un-proper property of the decoupler. In order to make the decoupler be proper and feasible, a second-order Maclaurin polynomial approximation is used to identify the final decoupling controller, referred to as a PI decoupler $\boldsymbol{D}_{\mathrm{PI}}(s)$.

$$\boldsymbol{D}_{\mathrm{PI}}(s)=\begin{bmatrix} 0.040\,64+\dfrac{3.477\times10^{-5}}{s} & -0.007\,66+\dfrac{0.000\,296}{s} & 1.054+\dfrac{0.021\,35}{s} \\ 0.001\,962-\dfrac{0.001\,962}{s} & \dfrac{0.000\,565\,2}{s} & 0 \\ -0.020\,72-\dfrac{3.871\times10^{-6}}{s} & -0.045\,93+\dfrac{0.000\,476}{s} & 6.326+\dfrac{0.128\,1}{s} \end{bmatrix}$$

Once the decoupler $\boldsymbol{D}_{\mathrm{PI}}(s)$ is determined, we need to check the validity of the approximation. The singular value plots of the decoupled open loop transfer matrix by decoupler $\boldsymbol{D}(s)$ and $\boldsymbol{D}_{\mathrm{PI}}(s)$ are shown in Fig. 1. The divergence of the singular value occurs at a frequency of 0.4 rad/s, so the dynamic behavior is the same as that at low frequencies ($\omega < 0.4$ rad/s). Thus, the tracking performance can be promised by the approximation.

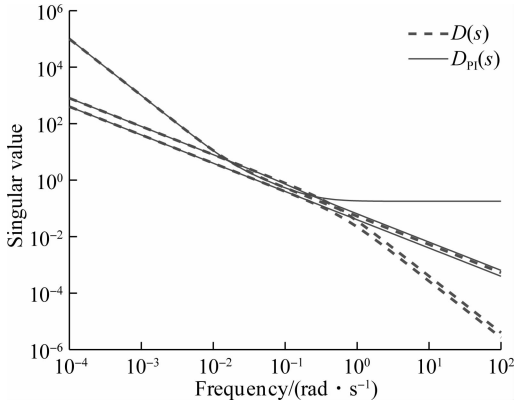

Fig. 1 Singular value plots of the decoupled open-loop transfer matrix by decouplers $\boldsymbol{D}(s)$ and $\boldsymbol{D}_{\mathrm{PI}}(s)$

2.2 MADRC design

If we put the achieved PI decoupler $\boldsymbol{D}_{\mathrm{PI}}(s)$ directly into practice, which plays a role of the centralized PID controller, the closed loop of the system can be stabilized by the decoupler. However, the control design seems overly ideal and unreliable, for which we add an extra control, having disturbance rejection capability, to the decoupled open-loop transfer function. The strategies, such as the DOB, unknown input observer (UIO) and ESO, can be chosen to the system. Among the above listed methods, the ESO needs the least plant information. Not only that, the ESO in combination with the PD controller is regarded as an effective control strategy in many fields. In Fig. 2, it is clear to see that the inputs of the ESO are the decoupler input and plant output for each loop. The decoupling error and the approximation error can be estimated by the ESO, and then compensated by the controller K.

Due to the second-order of the achieved decoupled open-loop transfer function in each loop, we formulize the generalized differential equation with the disturbance as follows:

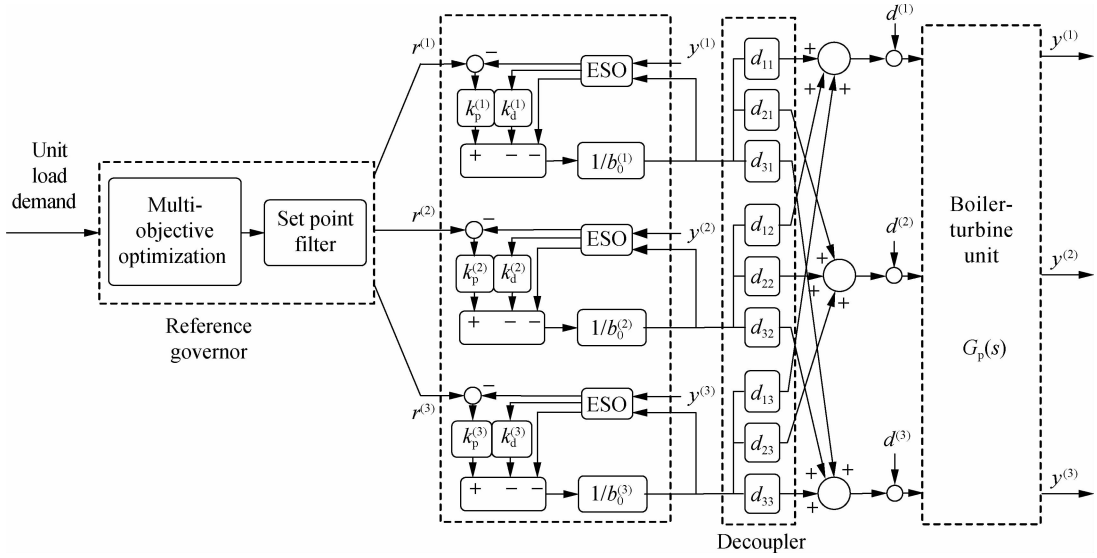

Fig. 2 Unity frame scheme of the control system

$$\ddot{y}(t) + a_1\dot{y}(t) + a_0 y(t) = b_1\dot{u}(t) + b_0 u(t) + f(y(t), u(t), d(t)) \tag{7}$$

where $f(y(t), u(t), d(t))$ is deemed as a lumped disturbance coming from the internal uncertainties and external disturbance of the model.

Assumption 1[10] The lumped disturbance $f(t)$ is differential and the value is constant in steady state, i. e., $\lim_{t\to\infty}\dot{f}(t) = 0$.

In the design of ADRC, an ESO is the main item used to estimate the lumped disturbance $f(y(t), u(t), d(t))$. Assuming that the state vector of Eq. (7) is $\boldsymbol{x} = [x_1 \quad x_2]^{\mathrm{T}}$, then, $x_3 = f$ is an augmented state.

Considering Assumption 1, we denote $\dot{f}$ as h. Then, the state-space equation (7) is

$$\dot{\boldsymbol{x}} = \boldsymbol{A}\boldsymbol{x} + \boldsymbol{B}u + \boldsymbol{E}h, \quad y = \boldsymbol{C}\boldsymbol{x} \tag{8}$$

where

$$\boldsymbol{A} = \begin{bmatrix} 0 & 1 & 0 \\ -a_0 & -a_1 & 1 \\ 0 & 0 & 0 \end{bmatrix}, \ \boldsymbol{B} = \begin{bmatrix} 0 \\ b_0 \\ 0 \end{bmatrix}, \ \boldsymbol{E} = \begin{bmatrix} 0 \\ 0 \\ 1 \end{bmatrix}$$

and $\boldsymbol{C} = [1 \quad b_1/b_0 \quad 0]$, $\boldsymbol{x} = [x_1 \quad x_2 \quad x_3]^{\mathrm{T}}$.

Then, the ESO with the full-order Luenberger is defined as below:

$$\dot{\boldsymbol{z}} = \boldsymbol{A}\boldsymbol{z} + \boldsymbol{B}u + \boldsymbol{L}_o(y - \hat{y}), \quad \hat{y} = \boldsymbol{C}\boldsymbol{z} \tag{9}$$

where the vector $\boldsymbol{z} = [z_1 \quad z_2 \quad z_3]^{\mathrm{T}}$ expresses the estimated state $\boldsymbol{x} = [x_1 \quad x_2 \quad x_3]^{\mathrm{T}}$ and $\boldsymbol{L}_o$ is the observer gain vector given as

$$\boldsymbol{L}_o = [\beta_1 \quad \beta_2 \quad \beta_3]^{\mathrm{T}} \tag{10}$$

Referring to Ref. [8], suppose that the bandwidth $\boldsymbol{\omega}_o$ of the observer is given, and the observer gain $\boldsymbol{L}_o$ can be calculated by Ackerman's formula as

$$\boldsymbol{L}_o = \psi(\boldsymbol{A}) \begin{bmatrix} \boldsymbol{C} \\ \boldsymbol{C}\boldsymbol{A} \\ \boldsymbol{C}\boldsymbol{A}^2 \end{bmatrix}^{-1} \begin{bmatrix} 0 \\ 0 \\ 1 \end{bmatrix} \tag{11}$$

where $\psi(\boldsymbol{A}) = (s + \omega_o)^3$.

Supposing that the designed ESO is well tuned, the estimated states z_1, z_2 and z_3 can track y, $\dot{y}$ and f, respectively. The augment state z_3 is essential to the control design, then the control law can be constructed as

$$u = u_0 - \frac{z_3}{\hat{b}} \tag{12}$$

where u_0 is the PD controller output, and $\hat{b}$ is the approximation of b_0.

Combining Eq. (7) with Eq. (12), the original differential equation is reduced to

$$\ddot{y}(t) + a_1\dot{y}(t) + a_0 y(t) = b_1\dot{u}_0(t) + b_0 u_0(t) - \frac{b_1}{b_0}\dot{z}_3 \tag{13}$$

According to Assumption 1, Eq. (13) is reduced to

$$\ddot{y}(t) + a_1\dot{y}(t) + a_0 y(t) = b_1\dot{u}_0(t) + b_0 u_0(t) \tag{14}$$

Taking the Laplace transformation, we can achieve the linear time invariant (LTI) transfer function as

$$G_o(s) = \frac{b_1 s + b_0}{s^2 + a_1 s + a_0} \tag{15}$$

In conclusion, the general plant can be compensated to become a LTI system by cancelling the lumped disturbance which is estimated by the ESO. Thus, the diagonal element of decoupled transfer matrix (4) can be regarded as the LTI model in each loop, despite the existence of a

decoupling error and other disturbances.

To design the feedback controller for the closed loop, we transform Eq. (15) into a space-state equation:

$$\dot{\boldsymbol{x}} = \boldsymbol{A}_{\mathrm{L}}\boldsymbol{x} + \boldsymbol{B}_{\mathrm{L}}u_0, \quad \boldsymbol{y} = \boldsymbol{C}_{\mathrm{L}}\boldsymbol{x} \tag{16}$$

where

$$\boldsymbol{A}_{\mathrm{L}} = \begin{bmatrix} 0 & 1 \\ -a_0 & -a_1 \end{bmatrix}, \ \boldsymbol{B}_{\mathrm{L}} = \begin{bmatrix} 0 \\ b_0 \end{bmatrix}, \ \boldsymbol{C}_{\mathrm{L}} = [1 \quad b_1/b_0]$$

It is interesting to note that the derived LTI model (16) can be used to design the feedback controller. Only considering the characteristic equation (15), the pole assignment method can be adopted here to replace the closed-loop poles. It is necessary to select the poles by taking full account of the dynamics in each loop. For simplicity, if the poles are placed at $-\omega_{\mathrm{c}}(\omega_{\mathrm{c}}>0)$, then the characteristic equation will be tuned to

$$s^2 + (a_1 + b_0k_2)s + (a_0 + b_0k_1) = (s+\omega_{\mathrm{c}})^2 \tag{17}$$

where k_1 and k_2 are the feedback gains.

Calculating from Eq. (17), we have

$$k_1 = \frac{\omega_{\mathrm{c}}^2 - a_0}{b_0}, \ k_2 = \frac{2\omega_{\mathrm{c}} - a_1}{b_0}$$

Then, the feedback controller gain is defined as

$$\boldsymbol{K} = [k_1 \quad k_2], \ \boldsymbol{u}_0 = \boldsymbol{K}[r - x_1 \quad x_2]^{\mathrm{T}}$$

Taking the Laplace transformation of the designed closed loop, the transfer function is obtained as

$$\boldsymbol{G}_{\mathrm{c}}(s) = \frac{Y(s)}{R(s)} = \frac{\frac{\omega_{\mathrm{c}}^2 - a_0}{b_0}(b_1 s + b_0)}{s^2 + 2\omega_{\mathrm{c}}s + \omega_{\mathrm{c}}^2} \tag{18}$$

When the closed-loop system enters a steady state ($s \to 0$), Eq. (18) can be expressed as

$$\boldsymbol{G}_{\mathrm{c}}(0) = \frac{\omega_{\mathrm{c}}^2 - a_0}{\omega_{\mathrm{c}}^2} \tag{19}$$

It is clear to see that if $a_0 \neq 0$, there will be a tracking offset on the output of the system, which should be compensated in the reference governor. Thus, a setpoint filter is placed behind the multi-objective optimization, whose static gain is $G_{\mathrm{c}}^{-1}(0)$, as shown in Fig. 2. Without loss of generality, the one-order low-pass filter is chosen as the set-point filter whose bandwidth can be set to be the same as that of the closed-loop transfer function in each loop.

2.3 Reference governor design

In general, the reference governor often plays a role of the feedforward controller, whose outputs are the well-designed setpoints to meet various constraints of the system. For the boiler-turbine, the fuel consumption, tracking performance, and other objectives should be considered. In addition, the proposed decoupling control should be constrained in a safety operation. So, a steady-state multi-objective optimization is a good choice for the reference governor design.

Suppose that the unit load demand E_{uld} is provided by AGC or operator in advance, then the steam pressure can be chosen according to the objective function:

$$\min_{x_{\mathrm{s}}} J = \beta_1 J_1(x_{\mathrm{s}}, u_{\mathrm{s}}) + \beta_2 J_2(x_{\mathrm{s}}, u_{\mathrm{s}}) + \beta_3 J_3(x_{\mathrm{s}}, u_{\mathrm{s}})$$

s. t.

$$\left.\begin{aligned} u_{1,\mathrm{s}} &= (0.0018u_{2,\mathrm{s}}x_{1,\mathrm{s}}^{9/8} + 0.15u_{3,\mathrm{s}})/0.9 \\ u_{2,\mathrm{s}} &= (0.16x_{1,\mathrm{s}}^{9/8} + x_{2,\mathrm{s}})/(0.73x_{1,\mathrm{s}}^{9/8}) \\ u_{3,\mathrm{s}} &= ((1.1u_{2,\mathrm{s}} - 0.19)x_{1,\mathrm{s}})/141 \end{aligned}\right\} \tag{20a}$$

$$u_{i,\min} \leqslant u_{i,\mathrm{s}} \leqslant u_{i,\max} \tag{20b}$$

$$x_{1,\min} \leqslant x_{1,\mathrm{s}} \leqslant x_{1,\max} \tag{20c}$$

$$x_{2,\mathrm{s}} = E_{\mathrm{uld}} \tag{20d}$$

where $J_1(x_{\mathrm{s}}, u_{\mathrm{s}}) = |x_{1,\mathrm{s}} - P_{\mathrm{typical}}|$ represents the drum pressure deviation from the desired steady state to the typical point; $J_2(x_{\mathrm{s}}, u_{\mathrm{s}}) = u_{1,\mathrm{s}}$ represents the energy consumption through the fuel valve; and $J_3(x_{\mathrm{s}}, u_{\mathrm{s}}) = -u_{2,\mathrm{s}}$ represents the pressure drop through the stream control valve which is required to keep open as wide as possible. The constraint (20a) is obtained from the model (1) under the assumption that the plant is in a steady state. The constraints (20b) and (20c) are obtained from the safety operation condition of $\boldsymbol{E}_{\mathrm{uld}}$, as shown in Fig. 3.

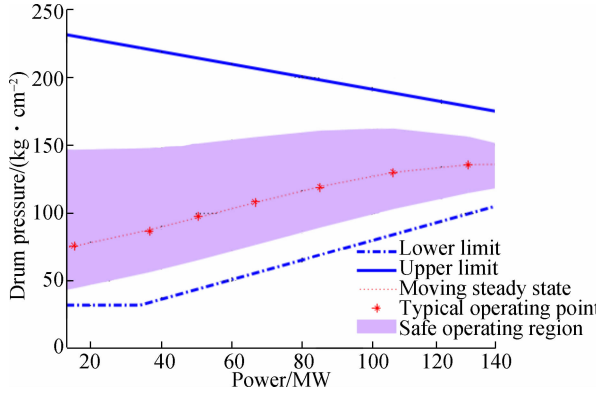

Fig. 3 Power-drum pressure operating window

From Fig. 3, the lower limit and upper limit are achieved through many experiments, while the safety region around the typical operation points is the constraint condition that we expect. According to the safety region, we can calculate constraints (20c) and (20b) at a specified $\boldsymbol{E}_{\mathrm{uld}}$.

With the help of Yalmip tool for nonlinear optimization, we can obtain the optimized steady state x_{s}, then

the setpoints represented as $[y_{1,s} \quad y_{2,s} \quad 0]^T$ can be achieved. Note that we want to keep the water level of the drum (i. e., the third output setpoint) at 0 m for the safety operation.

In conclusion, from the multi-objective optimization, the desired set points are found for the safety operation. Thus, the tracking control is implemented in the neighbor of the typical operating points. Its merits are that the nonlinearity of the model can be controllable and that the decoupling error is constrained in a predetermined range. Not only that, various objectives for the production can be met in a safe mode.

3 Simulation

In this part, we carry out the simulations on the boiler-turbine unit for the purpose of testing disturbance rejection ability and optimal tracking performance in a wide operation range. The parameters are shown in Tab. 2.

Tab. 2 Controller parameters rad/s

Loop No.	Feedback controller ω_c	ESO ω_o
1	7.0×10^{-2}	4.2×10^{-1}
2	11.0×10^{-2}	5.5×10^{-1}
3	2.3×10^{-2}	9.2×10^{-2}

3.1 Simulation of disturbance rejection ability

In this part, it is supposed that the boiler-turbine is stabilized at operating point 6#, then at $t = 150$ s, and an unknown disturbance $d = 0.3$ acts on fuel flow valve, reflecting fuel quality variation. Then, at $t = 600$ s, severe plant behavior occurs, where the parameters of model (1) shrink to 60% of its original value, reflecting the model mismatch problem. To compare with other methods, the conventional PID[5] and MPC with integral action (MPC-integral)[6] are adopted for the boiler-turbine unit. As shown in Fig. 4, the disturbance rejection ability of the proposed approach is significantly better than that of the other two methods.

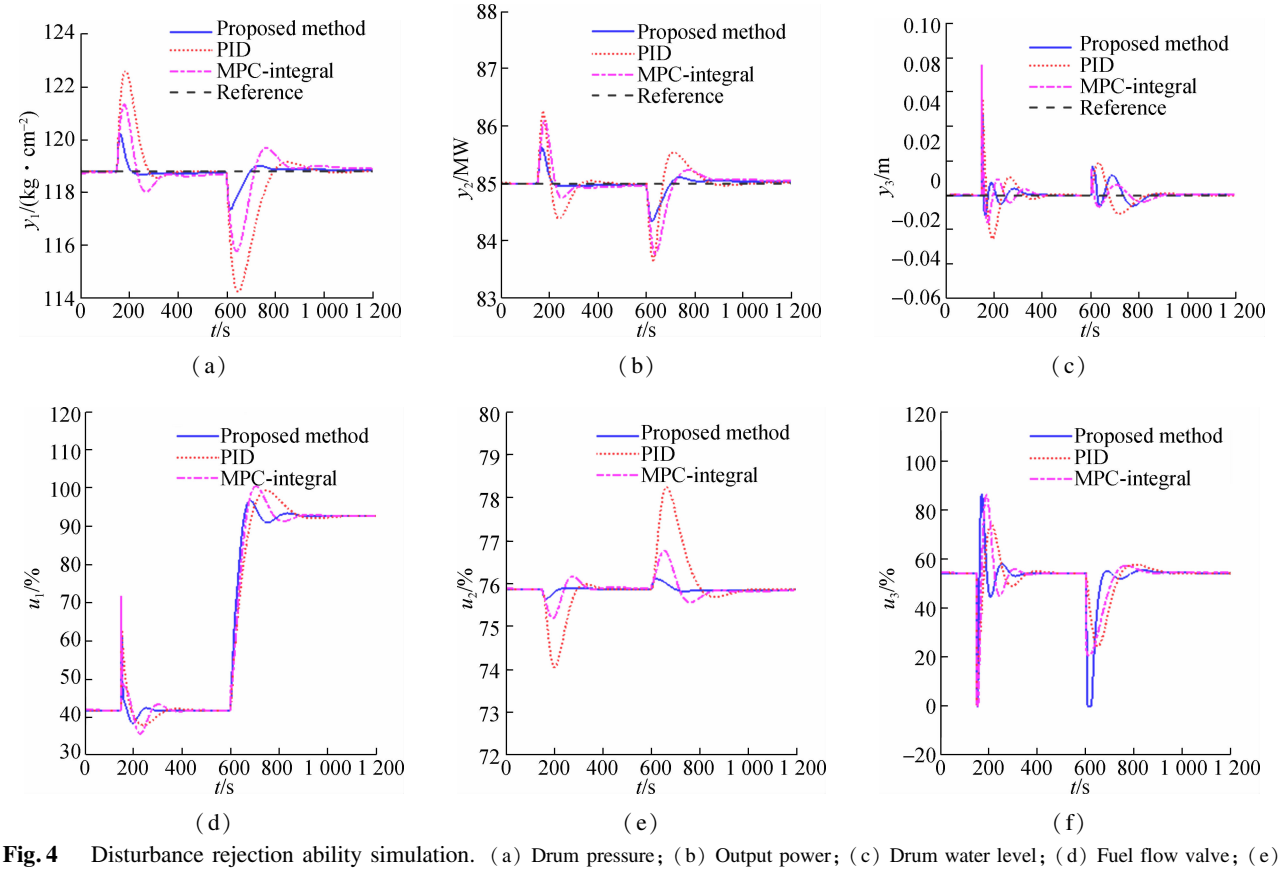

Fig. 4 Disturbance rejection ability simulation. (a) Drum pressure; (b) Output power; (c) Drum water level; (d) Fuel flow valve; (e) Steam control valve; (f) Feedwater control valve

3.2 Simulation of wide operation range

In this part, we aim at illustrating the multi-objective optimization for various requirements of the production. Suppose that the unit load demand is provided from AGC in advance, and two cases are presented with the same power setpoints.

Case 1 The only objective function J_1 is considered, reflecting a strict safe operation condition.

Case 2 The whole objective function J is considered, reflecting the composite performance of the optimization, where the weights are set to be $\beta_1 = 0.01$, $\beta_2 = 10$ and $\beta_3 = 1$.

From Fig. 5, we can see that the tracking performance

of the two cases is excellent, where the drum pressure setpoints of Case 1 are obtained around the typical operating points while Case 2 shows different drum pressure setpoints obtained from the reference governor. It is clear to see that Case 2 focuses on the multi-objective optimization, where the fuel consumption u_1 is lower than that of Case 1 and the steam control valve is kept open as wide as possible during the transition of operation. In both cases, the drum water is kept at 0 m for the safety operation.

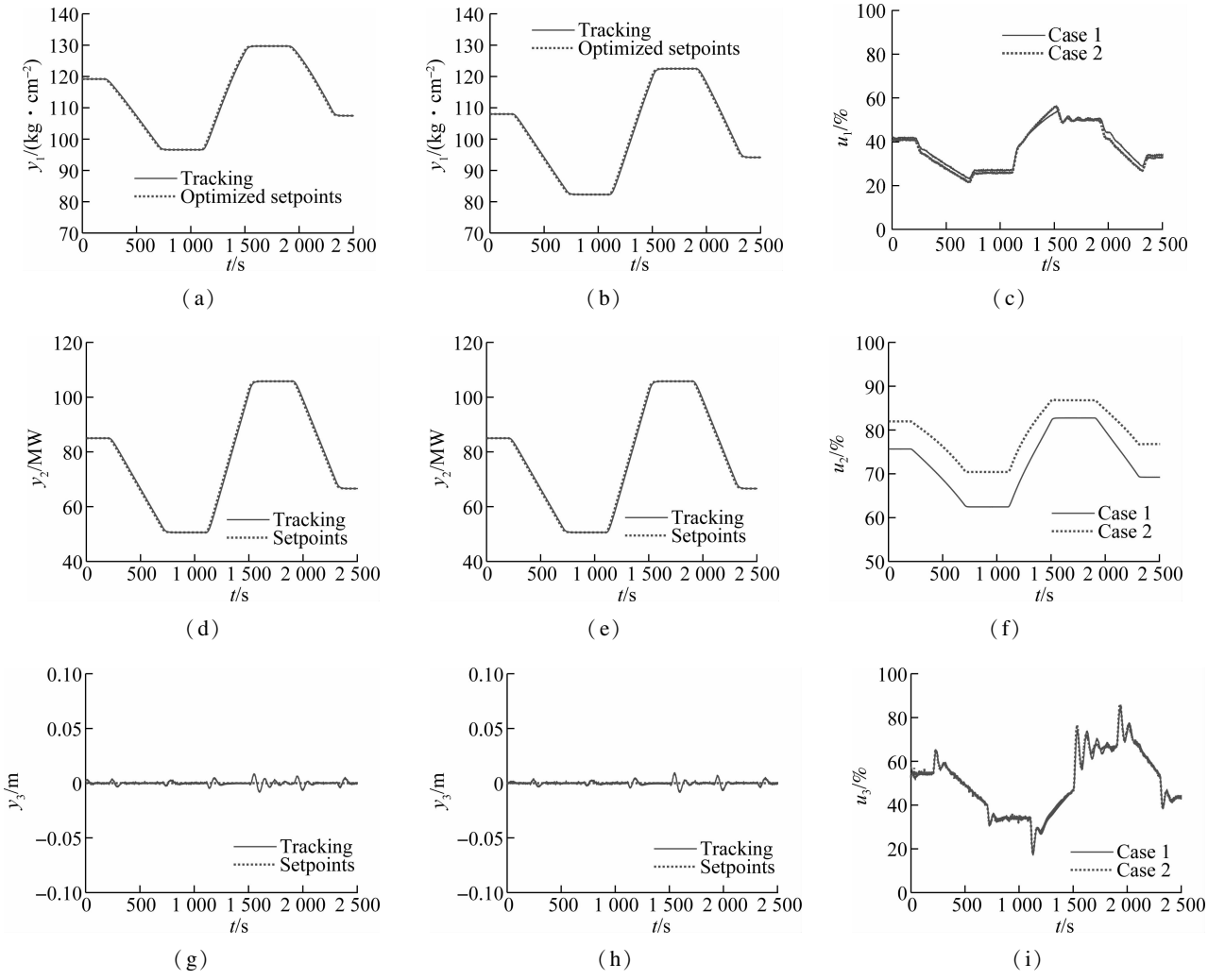

Fig. 5 System response for the multi-objective optimization in a wide operating range (a) Drum pressure of Case 1; (b) Drum pressure of Case 2; (c) Fuel flow valve; (d) Output power of Case 1; (e) Output power of Case 2; (f) Steam control valve; (g) Drum water level of Case 1; (h) Drum water level of Case 2; (i) Feedwater control valve

4 Conclusion

In this paper, a model-assisted ADRC with decoupling control is applied to the boiler-turbine unit system. The model uncertainties, decoupling errors and external disturbances are estimated by ESO, and compensated by the feedback controller. Not only that, the multi-objective optimization applied in the reference governor can satisfy the requirements of safety operation and energy conservation.

References

[1] Sun L, Hua Q S, Li D H, et al. Direct energy balance based active disturbance rejection control for coal-fired power plant[J]. *ISA Transactions*, 2017, **70**: 486 −493. DOI:10.1016/j.isatra.2017.06.003.

[2] Sun L, Li D H, Hu K T, et al. On tuning and practical implementation of active disturbance rejection controller: A case study from a regenerative heater in a 1000 MW power plant[J]. *Industrial & Engineering Chemistry Research*, 2016, **55**(23): 6686 − 6695. DOI: 10.1021/acs.iecr.6b01249.

[3] Chen P C, Shamma J S. Gain-scheduled ℓ1-optimal control for boiler-turbine dynamics with actuator saturation [J]. *Journal of Process Control*, 2004, **14**(3): 263 − 277. DOI:10.1016/S0959-1524(03)00040-4.

[4] Dettori S, Iannino V, Colla V, et al. An adaptive fuzzy logic-based approach to PID control of steam turbines in solar applications[J]. *Applied Energy*, 2018, **227**: 655 − 664. DOI:10.1016/j.apenergy.2017.08.145.

[5] Tan W, Marquez H J, Chen T W, et al. Analysis and control of a nonlinear boiler-turbine unit [J] *Journal of Process Control*, 2005, **15**(8): 883 − 891. DOI: 10.1016/j.jprocont.2005.03.007.

[6] Zhang R D, Xue A K, Wang S Q, et al. An improved

model predictive control approach based on extended nonminimal state space formulation[J]. *Journal of Process Control*, 2011, **21**(8): 1183 - 1192. DOI:10.1016/j.jprocont.2011.06.009.

[7] Wu X, Shen J, Li Y G, et al. Data-driven modeling and predictive control for boiler-turbine unit using fuzzy clustering and subspace methods[J]. *ISA Transactions*, 2014, **53**(3): 699 - 708. DOI:10.1016/j.isatra.2013.12.033.

[8] Fu C F, Tan W. Decentralized active disturbance rejection control for a benchmark boiler[C]// 2015 *IEEE 10th Conference on Industrial Electronics and Applications* (*ICIEA*). Auckland, New Zealand, 2015: 15617278. DOI:10.1109/ICIEA.2015.7334364.

[9] Wu X, Shen J, Li Y G, et al. Hierarchical optimization of boiler-turbine unit using fuzzy stable model predictive control[J]. *Control Engineering Practice*, 2014, **30**: 112 - 123. DOI:10.1016/j.conengprac.2014.03.004.

[10] Zhang F, Wu X, Shen J. Extended state observer based fuzzy model predictive control for ultra-supercritical boiler-turbine unit[J]. *Applied Thermal Engineering*, 2017, **118**: 90 - 100. DOI:10.1016/j.applthermaleng.2017.01.111.

[11] Han J Q. From PID to active disturbance rejection control[J]. *IEEE Transactions on Industrial Electronics*, 2009, **56**(3): 900 - 906. DOI:10.1109/tie.2008.2011621.

[12] Shao X L, Wang H L. Back-stepping active disturbance rejection control design for integrated missile guidance and control system via reduced-order ESO[J]. *ISA Transactions*, 2015, **57**: 10 - 22. DOI:10.1016/j.isatra.2015.02.013.

[13] Wu J S, Chen S L, He Z R, et al. On disturbance rejection of load simulator using model-based ESO[C]//2018 *IEEE 14th International Conference on Control and Automation* (*ICCA*). Anchorage, AK, USA, 2018. DOI: 10.1109/ICCA.2018.8444356.

[14] Nguyen H T, Jung J W. Disturbance-rejection-based model predictive control: Flexible-mode design with a modulator for three-phase inverters[J]. *IEEE Transactions on Industrial Electronics*, 2018, **65**(4): 2893 - 2903. DOI:10.1109/tie.2017.2758723.

[15] Zhao H R, Shen J, Li Y G, et al. A stable multi-objective economic MPC scheme for boiler-turbine units[J]. *IFAC—Papers on Line*, 2017, **50**(1): 11070 - 11075. DOI:10.1016/j.ifacol.2017.08.2489.

[16] Garrido J, Morilla F, Vazquez F. Centralized PID control by decoupling of a boiler-turbine unit[C]//2009 *European Control Conference* (*ECC*). Budapest, Hungary, 2009: 15034773. DOI: 10.23919/ECC.2009.7075027.

机炉协调系统的扩增状态观测器解耦控制及多目标优化策略

朱建忠[1,2]　吴　啸[1]　沈　炯[1]

([1]东南大学能源热转换及其过程测控教育部重点实验室,南京 210096)
([2]南京工程学院电力工程学院,南京 211167)

摘要:面对机炉协调系统出现的未知外部扰动及模型失配问题,提出了基于模型参考的扩增状态观测器的解耦控制策略.其解耦补偿器被简化成可以付诸实施的 PI 形式的解耦器并在频域下得到验证.而且,解耦误差以及模型不确定性、外部扰动可以被该观测器估计出来,并通过反馈控制器加以补偿.为了降低解耦器对模型误差的敏感度,同时满足诸如安全生产操作、节能减排等更多目标,设计的参考管理器可将被控对象的跟踪设定值优化在平衡点附近.仿真结果表明,所提控制策略可以很好地抑制包含解耦误差在内的多种扰动,同时多目标优化策略可以满足以安全生产为前提的多种要求.

关键词:单元机组;扩增观测器;解耦控制;多目标优化

中图分类号:TK321